Computers and Concrete, *Vol. 20, No. 6 (2017) 711-718*
DOI: https://doi.org/10.12989/cac.2017.20.6.711

Theoretical and experimental analysis of wave propagation in concrete blocks subjected to impact load considering the effect of nanoparticles

Hassan Bakhshandeh Amnieh*[1] and Mohammad Saber Zamzam[2]

[1]*School of Mining, College of Engineering, University of Tehran, Iran*
[2]*Department of Mining Engineering, Faculty of Engineering, University of Kashan, Iran*

(Received April 24, 2017, Revised August 18, 2017, Accepted August 21, 2017)

Abstract. Nanotechnology is a new filed in concrete structures which can improve the mechanical properties of them in confronting to impact and blast. However, in this paper, a mathematical model is introduced for the concrete models subjected to impact load for wave propagation analysis. The structure is simulated by the sinusoidal shear deformation theory (SSDT) and the governing equations of the concrete model are derived by energy method and Hamilton's principle. The silicon dioxide (SiO_2) nanoparticles are used as reinforcement for the concrete model where the characteristics of the equivalent composite are determined using Mori-Tanaka approach. An exact solution is applied for obtaining the maximum velocity of the model. In order to validate the theoretical results, three square models with different impact point and Geophone situations are tested experimentally. The effect of different parameters such as SiO_2 nanoparticles volume percent, situation of the impact, length, width and thickness of the model as well as velocity, diameter and height of impactor are shown on the maximum velocity of the model. Results indicate that the theoretical and experimental dates are in a close agreement with each other. In addition, using from SiO_2 nanoparticles leads to increase in the stiffness and consequently maximum velocity of the model.

Keywords: concrete model; impact load; mathematical model; SiO_2 nanoparticles; experimental test

1. Introduction

As it is well known, the best way for impact analysis of concrete structures in military, civil and mineral industries is the experimental tests in real scale. In real scale due to the lack of sufficient knowledge from the environment, the effects of combine parameters and other items, the detail and exact analysis of the structure is impossible. However, the researchers use from the small-scale models for the exact analysis of the concrete structures subjected to impact load. Due to the high cost and time consuming of experimental tests, matching a mathematical model for theoretical analysis of the concrete structures is very important which the researchers should study about his field. Our purpose in this article is opening a new field in the mining engineering for theoretical analysis of the models under impact, blast and etc.

Experimental analysis of wave propagation in different structures has been studied by many authors. Boadu and Long (1996) investigated the effects of fractures on the seismic-wave velocity and attenuation of a rock using theoretical results and experimental data. The propagation characteristics of blast-induced shock waves in a jointed rock mass were monitored and studied by Wu *et al.* (1998). Cai and Zhao (2000) presented a theoretical study and the UDEC modeling on the effects of multiple parallel planar fractures on the apparent attenuation of normally incident one-dimensional elastic waves. Stress wave propagation through concrete was simulated by Yaman *et al.* (2006) using finite element analysis. The concrete medium was modeled as a homogeneous material with smeared properties to investigate and establish the suitable finite element analysis method (explicit versus implicit) and analysis parameters (element size, and solution time increment) also suitable for rigorous investigation. Wang *et al.* (2006) studied wave propagation of one-dimensional normally incident wave in rock mass containing no joint, a single joint and two parallel joints were conducted by Three Dimensional Distinct Element Codes (3DEC). The calibration work of universal distinct element code (UDEC) modeling on P-wave propagation across single linearly and nonlinearly deformable fractures was conducted by Zhao *et al.* (2008). An experimental study of stress wave propagation across filled rock joints was carried out by Li and Ma (2009) using a modified Split Hopkinson Pressure Bar (SHPB) apparatus. An analytical and experimental study on a longitudinal wave (P-wave) transmission normally across a filled rock joint was presented by Li *et al.* (2010). Based on the conservation of momentum at the wave fronts and the displacement discontinuity method, quantitative analysis for the interaction between obliquely incident P- or S-blast wave and a linear elastic rock joint was carried out by Li and Ma (2010). The interaction of a blast wave with a multilayered material was investigated by Petel *et al.* (2011) for the purpose of blast wave attenuation. In order to investigate the transmission and reflection of stress waves across joints, a fractal damage joint model was developed by Li *et al.* (2011) based on fractal damage theory, and the analytical solution for the coefficients of

*Corresponding author
E-mail: hbakhshandeh@ut.ac.ir

ISSN: 1598-8198 (Print), 1598-818X (Online)

transmission and reflection of stress waves across joints was derived from the fractal damage joint model. Thermal stress and pore pressure development in microwave heated concrete was studied by Akbarnezhad and Ong (2011). Wave propagation across single and multiple parallel joints filled with viscoelastic medium was examined by Zhu *et al.* (2012). Kurtulus *et al.* (2012) presented experimental studies in wave propagation across a jointed rock mass. Li *et al.* (2013) employed a thin-layer interface model for filled rock joints to analyze wave propagation across the jointed rock masses. In another work, Li *et al.* (2014) extended the thin-layer interface model (TLIM) for filled joints to analyze wave propagation obliquely across jointed rock masses. The dynamic fracture mechanism of blast-induced fracturing of rock mass around a blast hoe, two-dimensional (2D) distinct element method was used by Aliabadian *et al.* (2014). Wang *et al.* (2015) developed a theoretical model based on the analysis of interaction process between stress waves and a single open joint. Khatibinia *et al.* (2016) predicted the compressive and flexural strengths of self-compacting mortar (SCM) containing nano-SiO_2, nano-Fe_2O_3 and nano-CuO using wavelet–based weighted least squares-support vector machines (WLS-SVM) approach. Akköse *et al.* (2016) investigated arrival direction effects of travelling waves on non-linear seismic response of arch dams. Al-Rousan *et al.* (2017) investigated the feasibility of using polypropylene fibers to improve the impact resistance of reinforced concrete slabs.

To the best of the author knowledge, no research has been found in the literature for mathematical modeling of concrete models under impact load considering the effects of nanotechnology. However, in this paper, for the first time, a mathematical model is presented for wave propagation of concrete models reinforced with SiO_2 nanoparticles subjected to impact load. SSDT, energy method and Hamilton's principle are utilized for obtaining the governing equations. An exact solution is used for calculating the velocity of the structure. In addition, the theoretical results are validated with experimental test for the square models with two geophones for recording the velocity. The effect of different parameters such as SiO_2 nanoparticles volume percent, situation of the impact, length, width and thickness of the model as well as velocity, diameter and height of impactor are shown on the maximum velocity of the model.

2. Mathematical modeling

Consider a concrete cube reinforced with SiO_2 nanoparticles as depicted in Fig. 1 as follows.

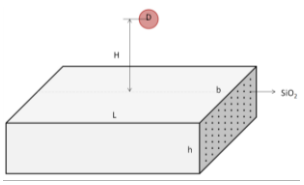

Fig. 1 A schematic figure for the concrete plate reinforced with SiO_2 nanoparticles under impact load

in which geometrical parameters of length L, width b and thickness h are indicated. The Cartesian coordinate is considered in the middle surface of plate in which x, y and z represent the axial, vertical and transverse directions, respectively. A particle with diameter of D is released from height of H on the sample.

2.1 Kinematic of theory

Here, the concrete cube is simulated with plate element based on SSDT where the displacement field can be obtained using as (Kolahchi *et al.* 2015)

$$u_1(x,\theta,z,t) = u(x,\theta,t) - z\frac{\partial w_b(x,\theta,t)}{\partial x} - f\frac{\partial w_s(x,\theta,t)}{\partial x}, \quad (1)$$

$$u_2(x,\theta,z,t) = v(x,\theta,t) - z\frac{\partial w_b(x,\theta,t)}{R\partial\theta} - f\frac{\partial w_s(x,\theta,t)}{R\partial\theta}, \quad (2)$$

$$u_3(x,\theta,z,t) = w_b(x,\theta,t) + w_s(x,\theta,t), \quad (3)$$

where $f = z - \frac{h}{\pi}\sin\frac{\pi z}{h}$; $w_b(x,\theta,t)$ and $w_s(x,\theta,t)$ are the bending and shear components of transverse displacement. The nonlinear kinematic relations can be expressed as follows

$$\varepsilon_{xx} = \frac{\partial u}{\partial x} - z\frac{\partial^2 w_b}{\partial x^2} - f\frac{\partial^2 w_s}{\partial x^2}, \quad (4)$$

$$\varepsilon_{\theta\theta} = \frac{\partial v}{R\partial\theta} + \frac{w_b}{R} + \frac{w_s}{R} - z\frac{\partial^2 w_b}{R^2\partial\theta^2} - f\frac{\partial^2 w_b}{R^2\partial\theta^2}, \quad (5)$$

$$\gamma_{\theta z} = p\frac{\partial w_s}{R\partial\theta} - \frac{v}{R}, \quad (6)$$

$$\gamma_{xz} = p\frac{\partial w_s}{\partial x}, \quad (7)$$

$$\gamma_{x\theta} = \frac{\partial u}{R\partial\theta} + \frac{\partial v}{\partial x} - 2z\frac{\partial^2 w_b}{R\partial x\,\partial\theta} - 2f\frac{\partial^2 w_s}{R\partial x\,\partial\theta}, \quad (8)$$

where $p = \cos\frac{\pi z}{h}$.

2.2 Mori-Tanaka model

In this section, the effective modulus of the concrete plate reinforced by SiO_2 nanoparticles is developed. Different methods are available to obtain the average properties of a composite. Due to its simplicity and accuracy even at high volume fractions of the inclusions, the Mori-Tanaka method (Mori and Tanaka 1973) is employed in this section. The matrix is assumed to be isotropic and elastic, with the Young's modulus E_m and the Poisson's ratio v_m. The constitutive relations for a layer of the composite with the principal axes parallel to the r, θ and

z directions are (Mori and Tanaka 1973)

$$\begin{Bmatrix}\sigma_{xx}\\ \sigma_{\theta\theta}\\ \sigma_{zz}\\ \tau_{\theta z}\\ \tau_{xz}\\ \tau_{x\theta}\end{Bmatrix}=\begin{bmatrix}k+m & l & k-m & 0 & 0 & 0\\ l & n & l & 0 & 0 & 0\\ k-m & l & k+m & 0 & 0 & 0\\ 0 & 0 & 0 & p & 0 & 0\\ 0 & 0 & 0 & 0 & m & 0\\ 0 & 0 & 0 & 0 & 0 & p\end{bmatrix}\begin{Bmatrix}\varepsilon_{xx}\\ \varepsilon_{\theta\theta}\\ \varepsilon_{zz}\\ \gamma_{\theta z}\\ \gamma_{xz}\\ \gamma_{x\theta}\end{Bmatrix}, \tag{9}$$

where σ_{ij}, ε_{ij}, γ_{ij}, k, m, n, l, p are the stress components, the strain components and the stiffness coefficients respectively. According to the Mori-Tanaka method the stiffness coefficients are given by (Mori and Tanaka 1973)

$$\begin{aligned}
k&=\frac{E_m\{E_m c_m+2k_r(1+\nu_m)[1+c_r(1-2\nu_m)]\}}{2(1+\nu_m)[E_m(1+c_r-2\nu_m)+2c_m k_r(1-\nu_m-2\nu_m^2)]}\\
l&=\frac{E_m\{c_m\nu_m[E_m+2k_r(1+\nu_m)]+2c_r l_r(1-\nu_m^2)]\}}{(1+\nu_m)[E_m(1+c_r-2\nu_m)+2c_m k_r(1-\nu_m-2\nu_m^2)]}\\
n&=\frac{E_m^2 c_m(1+c_r-c_m\nu_m)+2c_m c_r(k_r n_r-l_r^2)(1+\nu_m)^2(1-2\nu_m)}{(1+\nu_m)[E_m(1+c_r-2\nu_m)+2c_m k_r(1-\nu_m-2\nu_m^2)]}\\
&\quad+\frac{E_m[2c_m^2 k_r(1-\nu_m)+c_r n_r(1+c_r-2\nu_m)-4c_m l_r\nu_m]}{E_m(1+c_r-2\nu_m)+2c_m k_r(1-\nu_m-2\nu_m^2)}\\
p&=\frac{E_m[E_m c_m+2p_r(1+\nu_m)(1+c_r)]}{2(1+\nu_m)[E_m(1+c_r)+2c_m p_r(1+\nu_m)]}\\
m&=\frac{E_m[E_m c_m+2m_r(1+\nu_m)(3+c_r-4\nu_m)]}{2(1+\nu_m)\{E_m[c_m+4c_r(1-\nu_m)]+2c_m m_r(3-\nu_m-4\nu_m^2)\}}
\end{aligned} \tag{10}$$

where the subscripts m and r stand for matrix and reinforcement respectively. c_m and c_r are the volume fractions of the matrix and the nanoparticles respectively and k_r, l_r, n_r, p_r, m_r are the Hills elastic modulus for the nanoparticles (Mori and Tanaka 1973).

2.3 Governing equations

In this section, the energy method and Hamilton's principle are used for deriving the governing equations for the concrete plate reinforced by SiO_2 nanoparticles subjected to impact load. The potential energy of the structure can be written as

$$U=\frac{1}{2}\int\left(\sigma_{xx}\varepsilon_{xx}+\sigma_{\theta\theta}\varepsilon_{\theta\theta}+\tau_{x\theta}\varepsilon_{x\theta}+\tau_{xz}\varepsilon_{xz}+\tau_{\theta z}\varepsilon_{\theta z}\right)dV, \tag{11}$$

Substituting Eqs. (4) to (8) into Eq. (11) yields the potential energy of SSDT as follows

$$\begin{aligned}
U=0.5\int_A&\left(N_{xx}\left(\frac{\partial u}{\partial x}\right)+N_{\theta\theta}\left(\frac{\partial v}{R\partial\theta}+\frac{w_b}{R}+\frac{w_s}{R}\right)\right.\\
&+N_{x\theta}\left(\frac{\partial v}{\partial x}+\frac{\partial u}{R\partial\theta}\right)-Q_\theta\frac{v}{R}-M_{xx}\left(\frac{\partial^2 w_b}{\partial x^2}\right)\\
&-M_{\theta\theta}\left(\frac{\partial^2 w_b}{R^2\partial\theta^2}\right)-2M_{x\theta}\left(\frac{\partial^2 w_b}{R\partial\theta\partial x}\right)-S_{xx}\frac{\partial^2 w_s}{\partial x^2}\\
&\left.-S_{\theta\theta}\frac{\partial^2 w_s}{R^2\partial\theta^2}-2S_{x\theta}\frac{\partial^2 w_s}{R\partial\theta\partial x}+F_{\theta\theta}\frac{\partial w_s}{R\partial\theta}+F_{xx}\frac{\partial w_s}{\partial x}\right)dA,
\end{aligned} \tag{12}$$

where the resultant force and moments may be calculated as

$$\begin{bmatrix}N_{xx}\\ N_{\theta\theta}\\ N_{x\theta}\end{bmatrix}=\int_{-h/2}^{h/2}\begin{bmatrix}\sigma_{xx}\\ \sigma_{\theta\theta}\\ \tau_{x\theta}\end{bmatrix}dz, \tag{13}$$

$$\begin{bmatrix}M_{xx}\\ M_{\theta\theta}\\ M_{x\theta}\end{bmatrix}=\int_{-h/2}^{h/2}\begin{bmatrix}\sigma_{xx}\\ \sigma_{\theta\theta}\\ \tau_{x\theta}\end{bmatrix}z\,dz, \tag{14}$$

$$\begin{bmatrix}S_{xx}\\ S_{\theta\theta}\\ S_{x\theta}\end{bmatrix}=\int_{-h/2}^{h/2}\begin{bmatrix}\sigma_{xx}\\ \sigma_{\theta\theta}\\ \tau_{x\theta}\end{bmatrix}f\,dz, \tag{15}$$

$$\begin{bmatrix}F_{xx}\\ F_{\theta\theta}\end{bmatrix}=\int_{-h/2}^{h/2}\begin{bmatrix}\sigma_{xx}\\ \sigma_{\theta\theta}\end{bmatrix}p\,dz, \tag{16}$$

The kinetic energy of the structure is

$$K=\frac{\rho}{2}\int\left((\dot{u}_1)^2+(\dot{u}_2)^2+(\dot{u}_3)^2\right)dV, \tag{17}$$

where ρ is the density of the structure. The kinetic energy of SSDT can be obtained by substituting Eqs. (1)-(3) into Eq. (17) as follows

$$\begin{aligned}
K=0.5\int&\left(I_0\left(\left(\frac{\partial u}{\partial t}\right)^2+\left(\frac{\partial v}{\partial t}\right)^2+\left(\frac{\partial w_b}{\partial t}\right)^2+\left(\frac{\partial w_s}{\partial t}\right)^2+2\frac{\partial w_b}{\partial t}\frac{\partial w_s}{\partial t}\right)\right.\\
&-2I_1\left(\frac{\partial u}{\partial t}\frac{\partial^2 w_b}{\partial t\partial x}+\frac{\partial v}{\partial t}\frac{\partial^2 w_b}{R\partial t\partial\theta}\right)+I_2\left(\left(\frac{\partial^2 w_b}{\partial t\partial x}\right)^2+\left(\frac{\partial^2 w_b}{R\partial t\partial\theta}\right)^2\right)\\
&+I_3\left(\left(\frac{\partial^2 w_s}{\partial t\partial x}\right)^2+\left(\frac{\partial^2 w_s}{R\partial t\partial\theta}\right)^2\right)+2I_4\left(\frac{\partial^2 w_b}{\partial t\partial x}\frac{\partial^2 w_s}{\partial t\partial x}+\frac{\partial^2 w_b}{R\partial t\partial\theta}\frac{\partial^2 w_s}{R\partial t\partial\theta}\right)\\
&\left.+2I_5\left(\frac{\partial u}{\partial t}\frac{\partial^2 w_s}{\partial t\partial x}+\frac{\partial v}{\partial t}\frac{\partial^2 w_s}{R\partial t\partial\theta}\right)\right)dA.
\end{aligned} \tag{18}$$

where the moment of inertia in kinetic energy of three theories can be defined as

$$(I_0,I_1,I_2,I_3,I_4,I_5)=\int_{-h/2}^{h/2}\rho(1,z,z^2,f^2,zf,f)dz. \tag{19}$$

The work done by the impact load can be expressed as

$$W=\int qw\,dA. \tag{20}$$

where q can be written as (Gong and Lam 2000)

$$q=K_c^* u_3, \tag{21}$$

Where the effective stiffness of impactor (K_c^*) can be expressed as

$$\begin{aligned}
&K_C^*\\
&=\sqrt{\pi}\Gamma\left(\frac{P+1}{2}\right)\frac{2\Gamma\left(\frac{P}{2}+1\right)+\sqrt{\pi}\Gamma\left(\frac{P+1}{2}\right)}{4\Gamma^2\left(\frac{P}{2}+1\right)+\pi\Gamma^2\left(\frac{P+1}{2}\right)}\alpha_{max}^{P-1}K_{c,}
\end{aligned} \tag{22}$$

where Γ is gamma function; P is Hertzian indentation (usually P=1.5), $\alpha_{\max}$ is a parameter which can be written as

$$\alpha_{max}=\left(\frac{\bar{M}_{sand}.M_1}{\bar{M}_{sand}+M_1}\right)^{\frac{1}{(P+1)}}\left(\frac{P+1}{2}\right)^{\frac{1}{(P+1)}}\left(\frac{V_0^2}{K_c}\right)^{\frac{1}{(P+1)}} \tag{23}$$

where V_0 is the impact velocity of impactor and the contact stiffness (K_c) may be estimated as

$$K_c = \left(\frac{4}{3}\right) E R_I^{1/2}, \frac{1}{E} = \frac{1-\nu_1^2}{E_I} + \frac{1-\nu_P^2}{E_P} \tag{24}$$

where R_I, E_I and ν_I are radius, elastic modulus and poison's ratio of impactor, respectively; E_P and ν_p are elastic modulus and poison's ratio of structure, respectively.

The motion equations can be derived based on Hamilton's principle as follows

$$\int_0^t (\delta U - \delta W - \delta K) dt = 0. \tag{25}$$

Substituting Eqs. (12), (17) and (20) into Eq. (25) yields the CST motion equations as follows

$$\delta u: \quad \frac{\partial N_{xx}}{\partial x} + \frac{\partial N_{x\theta}}{R\partial\theta} = I_0 \frac{\partial^2 u}{\partial t^2}, \tag{26}$$

$$\delta v: \quad \frac{\partial N_{x\theta}}{\partial x} + \frac{\partial N_{\theta\theta}}{R\partial\theta} + \frac{Q_\theta}{R} = I_0 \frac{\partial^2 v}{\partial t^2}, \tag{27}$$

$$\begin{aligned} \delta w_b: \quad & \frac{\partial^2 M_{xx}}{\partial x^2} + \frac{\partial^2 M_{\theta\theta}}{R^2\partial\theta^2} + 2\frac{\partial^2 M_{x\theta}}{R\partial x\partial\theta} - \frac{N_\theta}{R} + q \\ & = I_0\left(\frac{\partial^2 w_b}{\partial t^2} + \frac{\partial^2 w_s}{\partial t^2}\right) - (I_2 + I_4)\left(\frac{\partial^4 w_b}{\partial t^2 \partial x^2} + \frac{\partial^4 w_b}{R^2 \partial t^2 \partial\theta^2}\right), \end{aligned} \tag{28}$$

$$\begin{aligned} \delta w_s: \quad & \frac{\partial^2 S_{xx}}{\partial x^2} + \frac{\partial^2 S_{\theta\theta}}{R^2\partial\theta^2} + 2\frac{\partial^2 S_{x\theta}}{R\partial x\partial\theta} + \frac{\partial F_{xx}}{\partial x} + \frac{\partial F_{\theta\theta}}{R\partial\theta} + q \\ & = I_0\left(\frac{\partial^2 w_b}{\partial t^2} + \frac{\partial^2 w_s}{\partial t^2}\right) - (I_3 + I_4)\left(\frac{\partial^4 w_s}{\partial t^2 \partial x^2} + \frac{\partial^4 w_s}{R^2 \partial t^2 \partial\theta^2}\right), \end{aligned} \tag{29}$$

However, combining Eqs. (13)-(16), (26)-(29), the motion equations may be obtained in terms of mechanical displacement as.

$$\begin{aligned} & A_{11}\frac{\partial^2 u}{\partial x^2} - B_{11}\left(\frac{\partial^3 w_b}{\partial x^3}\right) - E_{11}\left(\frac{\partial^3 w_s}{\partial x^3}\right) - B_{12}\left(\frac{\partial^3 w_b}{R^2\partial x\partial\theta^2}\right) \\ & + A_{12}\left(\frac{\partial^2 v}{R\partial x\partial\theta} + \frac{\partial w_b}{R\partial x} + \frac{\partial w_s}{R\partial x}\right) + \frac{A_{66}}{R}\left(\frac{\partial^2 u}{R\partial\theta^2} + \frac{\partial^2 v}{\partial x\partial\theta}\right) \\ & - \frac{B_{66}}{R}\left(2\frac{\partial^3 w_b}{R\partial x\partial\theta^2}\right) = I_0\frac{\partial^2 u}{\partial t^2} \end{aligned} \tag{30}$$

$$\begin{aligned} & A_{66}\left(\frac{\partial^2 u}{R\partial\theta\partial x} + \frac{\partial^2 v}{\partial x^2}\right) - B_{66}\left(2\frac{\partial^3 w_b}{R\partial x^2\partial\theta}\right) \\ & - E_{66}\left(2\frac{\partial^3 w_s}{R\partial x^2\partial\theta}\right) + \frac{A_{12}}{R}\left(\frac{\partial^2 u}{\partial x\partial\theta}\right) - \frac{B_{12}}{R}\left(\frac{\partial^3 w_b}{\partial x^2\partial\theta}\right) \\ & + \frac{A_{22}}{R}\left(\frac{\partial^2 v}{R\partial\theta^2} + \frac{\partial w_b}{R\partial\theta} + \frac{\partial w_s}{R\partial\theta}\right) - \frac{B_{22}}{R}\left(\frac{\partial^3 w_b}{R^2\partial\theta^3}\right) = I_0\frac{\partial^2 v}{\partial t^2} \end{aligned} \tag{31}$$

$$\begin{aligned} & B_{11}\frac{\partial^3 u}{\partial x^3} - D_{11}\left(\frac{\partial^4 w_b}{\partial x^4}\right) - H_{11}\left(\frac{\partial^4 w_s}{\partial x^4}\right) \\ & + B_{12}\left(\frac{\partial^3 v}{R\partial\theta\partial x^2} + \frac{\partial^2 w_b}{R\partial x^2} + \frac{\partial^2 w_s}{R\partial x^2}\right) - D_{12}\left(\frac{\partial^4 w_b}{R^2\partial\theta^2\partial x^2}\right) \\ & - H_{12}\left(\frac{\partial^4 w_s}{R^2\partial\theta^2\partial x^2}\right) + \frac{2B_{66}}{R}\left(\frac{\partial^3 u}{R\partial\theta^2\partial x} + \frac{\partial^3 v}{\partial x\partial\theta^2}\right) \\ & - \frac{2D_{66}}{R}\left(2\frac{\partial^4 w_b}{R\partial x^2\partial\theta^2}\right) - \frac{2H_{66}}{R}\left(2\frac{\partial^4 w_s}{R\partial x^2\partial\theta^2}\right) \\ & + \frac{B_{12}}{R^2}\frac{\partial^3 u}{\partial x\partial\theta^2} - \frac{D_{12}}{R^2}\left(\frac{\partial^4 w_b}{\partial x^2\partial\theta^2}\right) - \frac{H_{12}}{R^2}\left(\frac{\partial^4 w_s}{\partial x^2\partial\theta^2}\right) \\ & + \frac{B_{22}}{R^2}\left(\frac{\partial^3 v}{R\partial\theta^3} + \frac{\partial^2 w_b}{R\partial\theta^2} + \frac{\partial^2 w_s}{R\partial\theta^2}\right) - \frac{D_{22}}{R^2}\left(\frac{\partial^4 w_b}{R^2\partial\theta^4}\right) \\ & - \frac{H_{22}}{R^2}\left(\frac{\partial^4 w_s}{R^2\partial\theta^4}\right) - \frac{A_{12}}{R}\frac{\partial u}{\partial x} + \frac{B_{12}}{R}\left(\frac{\partial^2 w_b}{\partial x^2}\right) \\ & + \frac{H_{12}}{R}\left(\frac{\partial^2 w_s}{\partial x^2}\right) - \frac{A_{22}}{R}\left(\frac{\partial v}{R\partial\theta} + \frac{w_b}{R} + \frac{w_s}{R}\right) \\ & + \frac{B_{22}}{R}\left(\frac{\partial^2 w_b}{R^2\partial\theta^2}\right) + \frac{B_{22}}{R}\left(\frac{\partial^2 w_s}{R^2\partial\theta^2}\right) - K_c^* w_b \\ & = I_0\left(\frac{\partial^2 w_b}{\partial t^2} + \frac{\partial^2 w_s}{\partial t^2}\right) - (I_2 + I_4)\left(\frac{\partial^4 w_b}{tT^2\partial x^2} + \frac{\partial^4 w_b}{\partial t^2\partial\theta^2}\right) \end{aligned} \tag{32}$$

$$\begin{aligned} & L_{11}\left(\frac{\partial^3 u}{\partial x^3} + \left(\frac{\partial^2 w_b}{\partial x^2}\right)^2\right) - H_{11}\left(\frac{\partial^4 w_b}{\partial x^4}\right) - K_{11}\left(\frac{\partial^4 w_s}{\partial x^4}\right) \\ & + L_{12}\left(\frac{\partial^3 v}{R\partial\theta\partial x^2} + \frac{\partial^2 w_b}{R\partial x^2} + \frac{\partial^2 w_s}{R\partial x^2}\right) - H_{12}\left(\frac{\partial^4 w_b}{R^2\partial\theta^2\partial x^2}\right) \\ & - K_{12}\left(\frac{\partial^4 w_s}{R^2\partial\theta^2\partial x^2}\right) + \frac{2L_{66}}{R}\left(\frac{\partial^3 u}{R\partial\theta^2\partial x} + \frac{\partial^3 v}{\partial x\partial\theta^2}\right) \\ & - \frac{2H_{66}}{R}\left(2\frac{\partial^4 w_b}{R\partial x^2\partial\theta^2}\right) - \frac{2K_{66}}{R}\left(2\frac{\partial^4 w_s}{R\partial x^2\partial\theta^2}\right) + \frac{H_{12}}{R^2}\frac{\partial^3 u}{\partial x\partial\theta^2} \\ & - \frac{H_{12}}{R^2}\left(\frac{\partial^4 w_b}{\partial x^2\partial\theta^2}\right) - \frac{K_{12}}{R^2}\left(\frac{\partial^4 w_s}{\partial x^2\partial\theta^2}\right) + \frac{L_{22}}{R^2}\left(\frac{\partial^3 v}{R\partial\theta^3} + \frac{\partial^2 w_b}{R\partial\theta^2} + \frac{\partial^2 w_s}{R\partial\theta^2}\right) \\ & - \frac{H_{22}}{R^2}\left(\frac{\partial^4 w_b}{R^2\partial\theta^4}\right) - \frac{K_{22}}{R^2}\left(\frac{\partial^4 w_s}{R^2\partial\theta^4}\right) + L_{55}\left(\frac{\partial^2 w_s}{\partial x^2}\right) \\ & - G_{15p}\frac{\partial^2\varphi}{\partial x^2} + L_{44}\left(\frac{\partial^2 w_s}{R^2\partial\theta^2}\right) - K_c^* w_s \\ & = I_0\left(\frac{\partial^2 w_b}{\partial t^2} + \frac{\partial^2 w_s}{\partial t^2}\right) - (I_3 + I_4)\left(\frac{\partial^4 w_s}{tT^2\partial x^2} + \frac{\partial^4 w_s}{\partial t^2\partial\theta^2}\right) \end{aligned} \tag{33}$$

where

$$\begin{aligned} & (A_{11}, A_{12}, A_{22}, A_{44}, A_{55}, A_{66}) = \\ & \int_{-h/2}^{h/2} (Q_{11}, Q_{12}, Q_{22}, Q_{44}, Q_{55}, Q_{66}) dz, \end{aligned} \tag{34}$$

$$\begin{aligned} & (B_{11}, B_{12}, B_{22}, B_{66}) = \\ & \int_{-h/2}^{h/2} (Q_{11}, Q_{12}, Q_{22}, Q_{66}) z\, dz, \end{aligned} \tag{35}$$

$$\begin{aligned} & (L_{11}, L_{12}, L_{22}, L_{66}) = \\ & \int_{-h/2}^{h/2} (Q_{11}, Q_{12}, Q_{22}, Q_{66}) f\, dz, \end{aligned} \tag{36}$$

$$\begin{aligned} & (D_{11}, D_{12}, D_{22}, D_{66}) = \\ & \int_{-h/2}^{h/2} (Q_{11}, Q_{12}, Q_{22}, Q_{66}) z^2 dz, \end{aligned} \tag{37}$$

$$\begin{aligned} & (H_{11}, H_{12}, H_{22}, H_{66}) = \\ & \int_{-h/2}^{h/2} (Q_{11}, Q_{12}, Q_{22}, Q_{66}) zf dz, \end{aligned} \tag{38}$$

$$\left(K_{11},K_{12},K_{22},K_{66}\right)= \int_{-h/2}^{h/2}\left(Q_{11},Q_{12},Q_{22},Q_{66}\right)f^{2}dz\,, \tag{39}$$

$$\left(N_{44},N_{55}\right)=\int_{-h/2}^{h/2}\left(Q_{44},Q_{55}\right)pdz, \tag{40}$$

2.4 Solution

For harmonic wave propagation, the solution of equations of motion can be written in complex form as (Narendar and Gopalakrishnan 2012)

$$d\left(x,y,t\right)=d_0e^{i\left(k_1x-k_2y\right)+\omega t}\,,\quad d=u,v,w_b,w_s \tag{41}$$

where d_0, ω, k_2 and k_1 are the amplitudes of the wave motion, the circular frequency, the wave number in y-direction and the wave number in x-direction, respectively and $i=\sqrt{-1}$. By applying Eq. (41) into Eqs. (30)-(33), we have

$$\begin{bmatrix} P_{11} & P_{12} & P_{13} & P_{14} \\ P_{21} & P_{22} & P_{23} & P_{24} \\ P_{31} & P_{32} & P_{33} & P_{34} \\ P_{41} & P_{42} & P_{43} & P_{44} \end{bmatrix} \begin{Bmatrix} u \\ v \\ w_b \\ w_s \end{Bmatrix} = \begin{Bmatrix} 0 \\ 0 \\ 0 \\ 0 \end{Bmatrix}, \tag{42}$$

Finally, in order to obtain frequency, it is necessary to calculate the determinant of matrix and set it equal to zero. Finally, the velocity may be calculated from above relation.

3. Experimental test

As shown in Figs. 2(a)-2(c), three square concrete samples (70 cm×70 cm) are considered with 2 geophone with the distance of 10 cm for recording the velocity induced by the impact.

In Figs. 2(a)-2(c), 5, 4 and 3 impact points with the step of 10 cm are assumed where the distance of geophone 2 from the right side of the boundary is 5 cm, 15 cm and 25 cm, respectively. In three cases, a steel particle with the diameter of D=125 *mm* is released from height of H=20 *cm* on the sample. The main objective of these tests is obtaining the maximum velocity which is discussed in the next section (Pourghasemi Sagand 2015).

4. Numerical results and discussion

The material constants used in the calculation are: concrete cube with elastic modules of E_m=20 *GPa* and Poisson's ratio of v_m=0.3 and SiO_2 nanoparticles with elastic modules of E_r=75 *GPa* and Poisson's ratio of v_r=0.27. Based on the proposed method in section 2 and experimental test, the velocity of the structure is calculated.

4.1 Experimental results

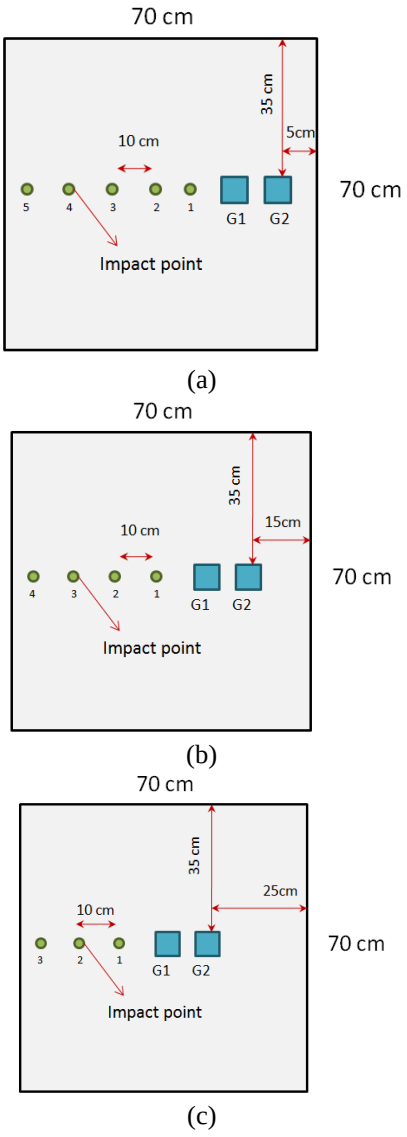

Fig. 2 The situation of geophones and impact points for experimental tests (a) case 1 (b) case 2 (c) case 3

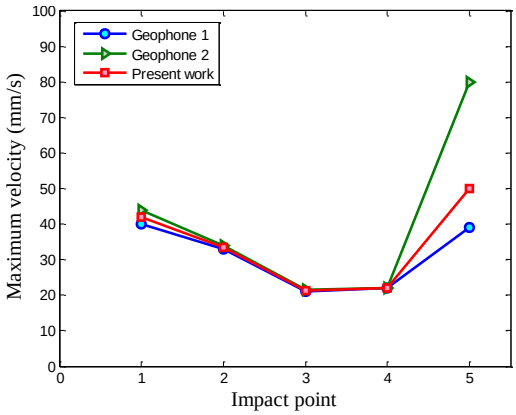

Fig. 3 Theoretical and experimental maximum velocity for different impact points of case 1

In case 1 (Fig. 2(a)), the geophones are near the left boundary in the symmetric line. The maximum velocities related to 5 impact points are shown in Fig. 3. As can be

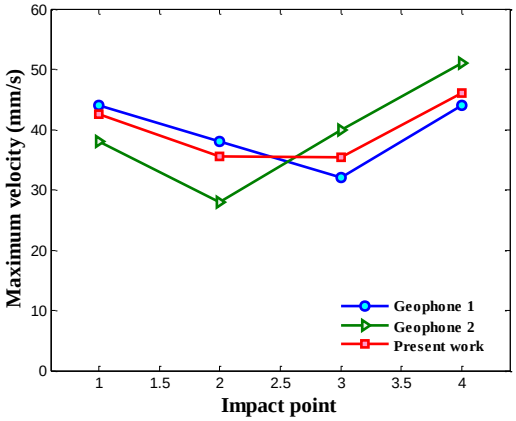

Fig. 4 Theoretical and experimental maximum velocity for different impact points of case 2

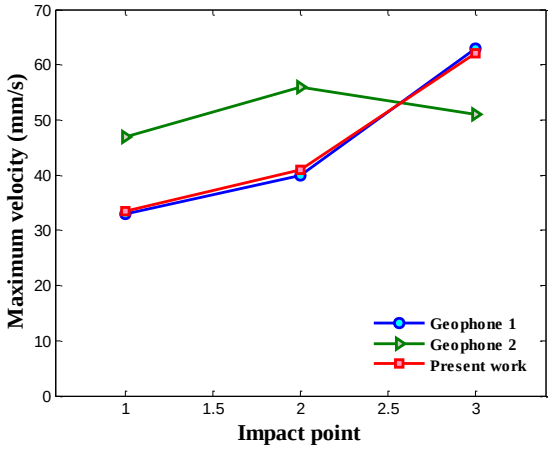

Fig. 5 Theoretical and experimental maximum velocity for different impact points of case 3

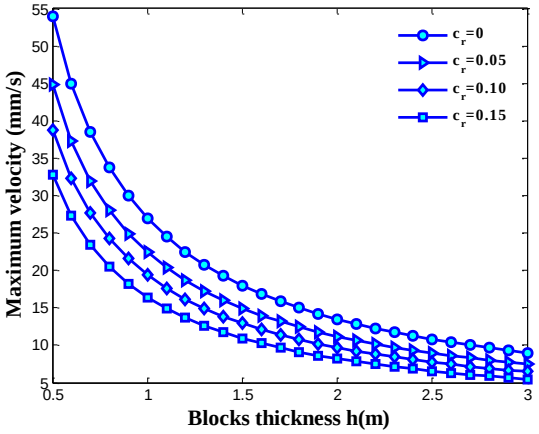

Fig. 6 The effect of SiO_2 nanoparticles on the maximum velocity versus structure length

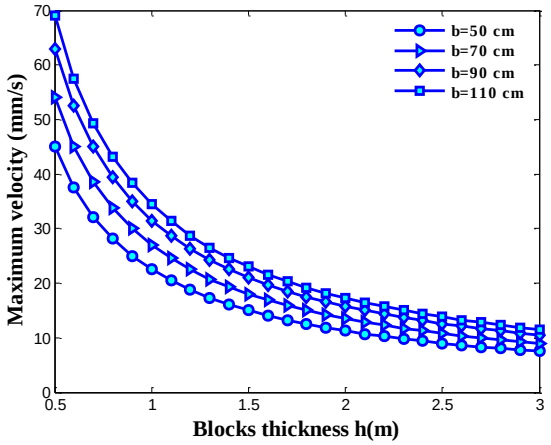

Fig. 7 The effect of structure width on the maximum velocity versus structure length

seen, the maximum velocity is decreased from impact point 1 to impact point 4 while it enhances at the impact point 5. It is since the impact point 5 is near the boundary of the structure and the reflected wave can increase the velocity of this point. In addition, the maximum velocity recorded by geophone 2 is higher than geophone 1 since the distance of geophone 2 from the left boundary is lower than that of geophone 1 and hence, the reflected wave from the boundary can amplify the maximum velocity.

In order to more accurate study of this problem, cases 2 and 3 (Figs. 2(b) and 2(c)) are considered where the distances of geophones from the left boundary are 15 cm and 25 cm, respectively. The maximum velocity related to cases 2 and 3 is illustrated in Figs. 4 and 5, respectively. It can be seen that in the impact points of 1 and 2, the maximum velocity recorded by geophone 2 is lower than that of geophone 1. It is due to the fact that in cases 2 and 3, the geophone 2 is further from the structure boundary and hence the effect of reflected wave and boundary decreases. This phenomenon is converse for the impact points of 3 and 4 in case 2 and impact point of 3 in case 3 so that the maximum velocity recorded by geophone 2 is higher than geophone 1. It is because the mentioned impact points are near the boundary of the structure and the effect of reflected wave will be increased.

However, the distance of geophones forms the boundary and the step of the impact points are important parameters which improve the accuracy of the results.

4.2 Validation

Before presenting the theoretical results, we should validate the applied model and the obtained results. However, considering the geometrical parameters of the structure as well as impactor diameter and height the same as experimental test, the maximum velocity of the structure is calculated. The results of present work are shown in Figs. 3-5 and compared with the experimental datas. It can be observed that the theoretical results are in a good agreement with the experimental datas. However, it can be concluded that the proposed method and solution method are appropriate for this problem.

4.3 Theoretical results

In this section, the effect of different parameters such as SiO_2 nanoparticles volume percent, situation of the impact, length, width and thickness of the model as well as velocity, diameter and height of the impactor are shown on the maximum velocity of the model.

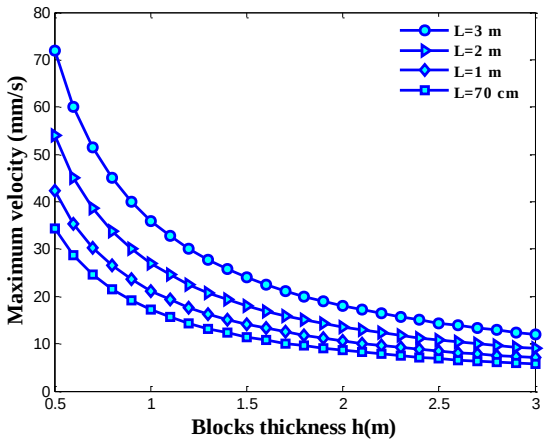

Fig. 8 The effect of structure length on the maximum velocity versus structure length

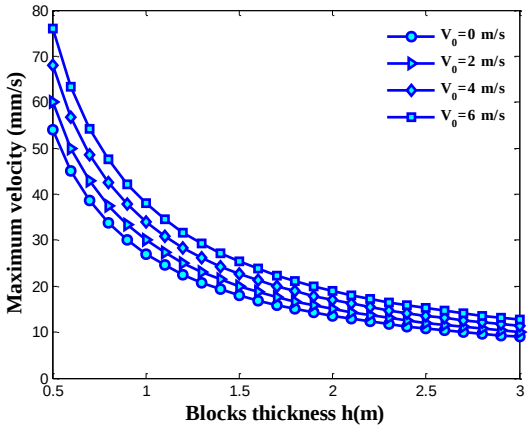

Fig. 9 The effect of impactor velocity on the maximum velocity versus structure length

In order to show the effect of SiO_2 nanoparticles volume percent in the maximum velocity versus the thickness of the structure, Fig. 6 is plotted. It is shown that with increasing the thickness of the structure, the maximum velocity decreases due to increase in the stiffness of the structure. It can be found that with increasing the volume percent of SiO_2 nanoparticles, the maximum velocity decreases. It is due to the fact that with increasing volume percent of SiO_2 nanoparticles, the stiffness of structure increases. However, the SiO_2 nanoparticles can improve the reaction of the structure in contact with the impact load.

The effects of the width and length of the structure on the maximum velocity versus the thickness of the structure are demonstrated in Figs. 7-9, respectively.

As can be seen, increasing the length and width of the structure causes to increase in the maximum velocity of the concrete structure. It is due to the fact that increasing the length and width of the structure leads to lower stiffness in the structure.

Figs. 10 and 11 present the effects of the velocity, diameter and height of the impactor on the maximum velocity versus the thickness of the structure, respectively. It is shown that the maximum velocity increases with increasing the velocity, diameter and height of the impactor. It is due to the fact that with increasing the velocity,

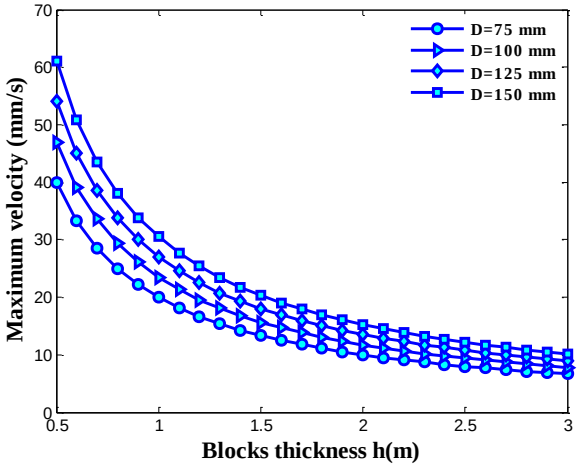

Fig. 10 The effect of impactor diameter on the maximum velocity versus structure length

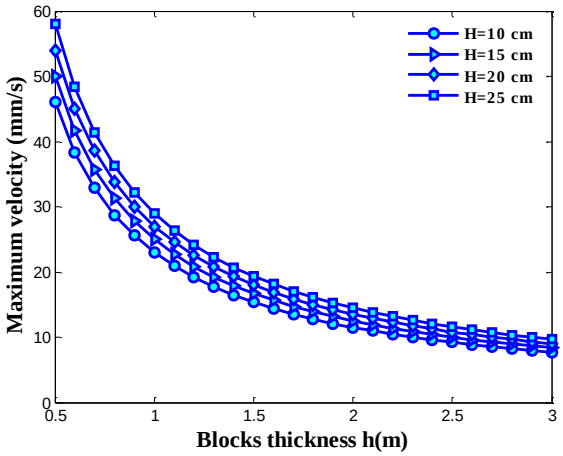

Fig. 11 The effect of impactor high on the maximum velocity versus structure length

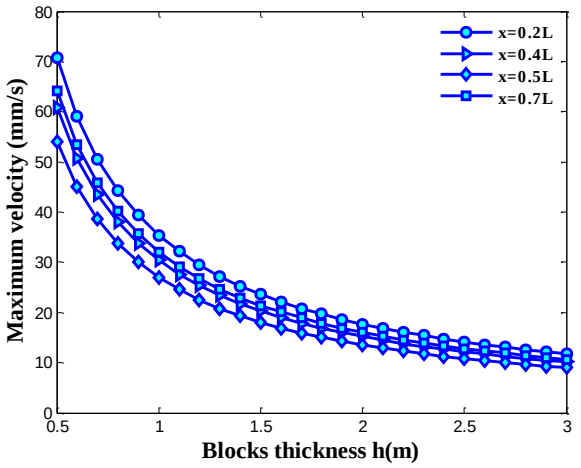

Fig. 12 The effect of impact point situation on the maximum velocity versus structure length

diameter and height of the impactor, the kinetic energy of the impactor increases.

The effect of the impact point situation, Fig. 12 is plotted where the maximum velocity changes with the thickness of the structure. It can be seen that the maximum

velocity for the points near the boundaries is higher than that of the middle point. It is physically reasonable since in the points near the boundaries, we have the effect of the reflected wave and hence the maximum velocity increases.

5. Conclusions

Theoretical an experimental wave propagation analysis in concrete plates were presented in this article. The structure was simulated with SSDT mathematically and the corresponding governing equations were derived using energy method and Hamilton's principle. Another novelty of this work was considering the effect of SiO_2 nanoparticles volume percent effect on the wave propagation behaviour of the structure based on Mori-Tanaka model. Based on exact solution, the maximum velocity of the structure was obtained and compared with the experimental datas. The effect of different parameters such as SiO_2 nanoparticles volume percent, length, width and thickness of the model as well as velocity, diameter and height of the impactor were shown on the maximum velocity of the model. Results indicate that the theoretical results were in a good agreement with the experimental datas. It was found that the maximum velocity for the impact points near the boundaries is higher than other points due to the effect of the reflected wave. It can be found that with increasing the volume percent of SiO_2 nanoparticles, the maximum velocity decreases. Increasing the length and width as well as decreasing the thickness of the structure causes to increase in the maximum velocity of the concrete structure. In addition, the maximum velocity increases with increasing the velocity, diameter and height of the impactor. Finally, it is hoped that this work open a new field in the mining engineering for mathematical modelling of the structure in order to predict the impact and blast response of them.

References

Akbarnezhad, A. and Ong, K.C.G. (2011), "Thermal stress and pore pressure development in microwave heated concrete", *Comput. Concrete*, **8**(4), 425-443.

Akköse, M. (2016), "Arrival direction effects of travelling waves on nonlinear seismic response of arch dams", *Comput. Concrete*, **18**(2), 179-199.

Aliabadian, Z., Sharafisafa, M., Mortazavi, A. and Maarefvand, P. (2014), "Wave and fracture propagation in continuum and faulted rock masses: Distinct element modeling", *Arab J. Geosci.*, **7**(12), 5021-5035.

Al-Rousan, R.Z., Alhassan, M.A. and Al-Salman, H. (2017), "Impact resistance of polypropylene fiber reinforced concrete two-way slabs", *Struct. Eng. Mech.*, **62**(3), 373-380.

Boadu, F.K. and Long, L.T. (1996), "Effects of fractures on seismic-wave velocity and attenuation", *Geophys. J. Int.*, **127**(1), 86-110.

Cai, J.G. and Zhao, J. (2000), "Effects of multiple parallel fractures on apparent attenuation of stress waves in rock masses", *J. Rock Mech. Min. Sci.*, **37**(4), 661-682.

COMSOL Inc (2013), http://www.comsol.com.

Gong, S.W. and Lam, K.Y. (2000), "Effects of structural damping and stiffness on impact response of layered structure", *AIAA J.*, **38**(9), 1730-1735.

Khatibinia, M., Feizbakhsh, A., Mohseni, E. and Ranjbar, M.M. (2016), "Modeling mechanical strength of self-compacting mortar containing nanoparticles using wavelet-based support vector machine", *Comput. Concrete*, **18**(6), 1065-1082.

Kolahchi, R., Moniri Bidgoli, A.M. and Heydari, M.M. (2015), "Size-dependent bending analysis of FGM nano-sinusoidal plates resting on orthotropic elastic medium", *Struct. Eng. Mech.*, **55**(5), 1001-1014.

Kurtulus, C., Uckardes, M., Sarı, U. and Guner, O. (2012), "Experimental studies in wave propagation across a jointed rock mass", *Bull. Eng. Geol. Environ.*, **71**(2), 231-234.

Li, J. and Ma, G. (2009), "Experimental study of stress wave propagation across a filled rock joint", *J. Rock Mech. Min. Sci.*, **46**(3), 471-478.

Li, J. and Ma, G. (2010), "Analysis of blast wave interaction with a rock joint", *Rock Mech. Rock Eng.*, **43**(6), 777-787.

Li, J., Ma, G. and Huang, X. (2010), "Analysis of wave propagation through a filled rock joint", *Rock Mech. Rock Eng.*, **43**(6), 789-798.

Li, J.C., Li, H.B., Jiao, Y.Y., Liu, Y.Q., Xia, X. and Yu, C. (2014), "Analysis for oblique wave propagation across filled joints based on thin-layer interface model", *J. Appl. Geophys.*, **102**, 39-46.

Li, J.C., Wu, W., Li, H.B., Zhu, J.B. and Zhao, J. (2013), "A thin-layer interface model for wave propagation through filled rock joints", *J. Appl. Geophys.*, **91**, 31-38.

Li, Y., Zhu, Z., Li, B., Deng, J. and Xie, H. (2011), "Study on the transmission and reflection of stress waves across joints", *J. Rock Mech. Min. Sci.*, **48**(3), 364-371.

Mori, T. and Tanaka, K. (1973), "Average stress in matrix and average elastic energy of materials with misfit ting inclusions", *Acta Metall. Mater.*, **21**(5), 571-574.

Narendar, S. and Gopalakrishnan, S. (2012), "Study of terahertz wave propagation properties in nanoplates with surface and small-scale effects", *J. Mech. Sci.*, **64**(1), 221-231.

Petel, O.E., Jetté, F.X., Goroshin, S., Frostm D.L. and Ouellet, S. (2011), "Blast wave attenuation through a composite of varying layer distribution", *Shock Wave.*, **21**(3), 215-224.

Pourghasemi Sagand, M. (2015), "The experimental study of the effects of discountinously on the blast-induced energy partitioning in resistant rocks", M.Sc. Dissertation, University of Tehran, Iran.

Wang, W., Hao, H., Li, X., Yan, Z. and Gong, F. (2015), "Effects of a single open joint on energy transmission coefficients of stress waves with different waveforms", *Rock Mech. Rock Eng.*, **48**(5), 2157-2166.

Wang, W.H., Li, X.B. Zuo, Y.J., Zhou, Z.L. and Zhang, Y.P. (2006), "3DEC modeling on effect of joints and interlayer on wave propagation", *Trans. Nonferr. Met. SOC. Chin.*, **16**(3), 728-734.

Wu, Y.K., Hao, H., Zhou, Y.X. and Chong, K. (1998), "Propagation characteristics of blast-induced shock waves in a jointed rock mass", *Soil Dyn. Earthq. Eng.*, **17**(6), 407-412.

Yaman, I.O., Akbay, Z. and Aktan, H. (2006), "Numerical modelling and finite element analysis of rnstress wave propagation for ultrasonic pulse velocity testing of concrete", *Comput. Concrete*, **3**(6), 423-437.

Zhao, X.B., Zhao, J., Cai, J.G. and Hefny, A.M. (2008), "UDEC modelling on wave propagation across fractured rock masses", *Comput. Geotech.*, **35**(1), 97-104.

Zhu, J.B., Zhao, X.B., Wu, W. and Zhao, J. (2012), "Wave propagation across rock joints filled with viscoelastic medium using modified recursive method", *J. Appl. Geophys.*, **86**, 82-87.

CC